SAND-77-1557
Unlimited Release
R-7

MICROSTRUCTURAL EVALUATION AND NON-DESTRUCTIVE EXAMINATION OF 2.25 Cr-1 Mo STEEL SUBJECTED TO ELEVATED TEMPERATURE CREEP AND FATIGUE DAMAGE

J. A. Van Den Avyle, W. B. Jones, J. H. Gieske

2900 Q(7-73)

Prepared for
U. S. NUCLEAR REGULATORY COMMISSION

SAND-77-1557
Unlimited Release

MICROSTRUCTURAL EVALUATION AND NON-DESTRUCTIVE EXAMINATION OF 2.25 Cr-1 Mo STEEL

J. A. Van Den Avyle
W. B. Jones
J. H. Gieske

Date Published: July 1978

Sandia Laboratories
Albuquerque, New Mexico 87185
operated by
Sandia Corporation
for the
U. S. Department of Energy

Prepared for
Division of Reactor Safety Research
Office of Nuclear Regulatory Research
U. S. Nuclear Regulatory Commission
Washington, D.C. 20555
Under Interagency Agreement DOE 40-550-75
NRC FIN No. A1172

ACKNOWLEDGEMENTS

R. E. Nickell, formerly of Division 5431 and currently at Pacifica Technology, Del Mar, CA, provided the initial program direction for this task.

J. C. Swearengen, Division 8316, performed the creep testing.

C. R. Hills, Division 5822, carried out the transmission electron microscopy.

ABSTRACT

A need exists for a volumetric non-destructive examination (NDE) technique which can measure changes in microstructure caused by elevated temperature creep and fatigue in structural materials used in advanced high temperature reactors. One example of such a material is 2.25 Cr-1 Mo steel which is used as steam generator tubing in current designs for advanced high temperature reactors. In this study specimens of 2.25 Cr-1 Mo steel were damaged to various levels by creep and combined creep-fatigue cycling at 886 K (1100°F) with hold periods. Ultrasonic shear wave velocity measurements were performed and showed small changes with large amounts of creep or fatigue damage; these changes were deemed too small for practical application. Measurements of magnetic properties were unsuccessful in following damage. Optical and transmission electron microscopy (TEM) were performed on the samples. TEM observations showed that microstructural changes which occurred at 886 K (1100°F) did not occur homogeneously throughout the matrix; during creep, carbide spheroidization and coarsening began in widely separated regions, with an increasing fraction of the material undergoing the process with time. A precipitate was observed to form during fatigue which did not occur during simple aging or creep.

CONTENTS

TABLES

ILLUSTRATIONS

1. Introduction

This report describes work performed for one task in an ongoing contract with the Nuclear Regulatory Commission* entitled "Elevated Temperature Design Assessment" (contract number 189A 1172). The purpose of the project is to quantify elevated temperature failure modes for materials used in LMFBR primary and secondary coolant loop components. This quantification is being attempted by making physical measurements of materials damaged at elevated temperature; these measurements include destructive examination by optical and transmission electron microscopy (TEM) and non-destructive examination (NDE) by ultrasonic, magnetization, and positron annihilation techniques.

Driven by the need to design for long-term, high-temperature service, a large program of research into creep-fatique interactions has been conducted in this country over the past several years. This program has included studies of material behavior, analysis procedures, and design criteria. However, uncertainties are still present, particularly regarding long-term prediction of behavior out to projected component life times (30 to 40 years). For this reason, there is strong interest in developing intermittent or continuous in-service inspection techniques to detect imminent creep-fatigue failure.

The purpose of the task described herein is to attempt to determine whether conventional non-destructive examination methods, as eddy current and ultrasonic techniques, can detect progressive

*This work was funded by the Division of Reactor Safety, Office of Nuclear Regulatory Research

creep-fatigue damage in a candidate material for an LMFBR steam generator--2.25 Cr-1 Mo steel. Understanding and predicting the mechanical behavior and failure modes of this material is important because of the potentially serious consequences of leakage of steam into liquid sodium.

The NDE techniques used here attempt to measure damage by following changes in microstructural features which occur during creep and fatigue deformation at elevated temperatures. These features include grain shape, texture, cell and subgrain size and shape, dislocation distribution, and second phase morphology. In addition, possible formation of internal flaws, such as grain boundary cracks or voids, were investigated; evaluation of NDE methods for surface crack detection was not not attempted here as there are large efforts elsewhere.

As a parallel effort to the NDE investigations, microstructural examination of the damaged specimens was carried out by optical and transmission electron microscopy. It was felt that these observations were required to correlate with NDE readings and to explain the mechanisms behind any positive NDE results. The TEM observations also provide data to assess the validity of a recent proposal by Hale [1] that with 2.25 Cr-1 Mo steel it is possible to directly relate measurements of microstructural changes to creep life fractions.

This report summarizes all work conducted on unwelded 2.25 Cr-1 Mo steel for the program and includes some early results previously published by R. E. Nickell [2] as an interim report. A report covering creep and fatigue damage of a 2.25 Cr-1 Mo steel weldment has also been published by J. A. Van Den Avyle [3].

2. Creep and Creep-Fatigue Testing

2.1 Experimental

A plate of 2.25 Cr-1 Mo steel was obtained with the aid of Dr. C. R. Brinkman of the Oak Ridge National Laboratory Metals and Ceramics Division. The piece was approximately 30 cm x 20 cm x 2.5 cm (12 in. x 8 in. x 1 in.) and came from a heat designated 3P5601. The chemistry of this heat is listed below and its room temperature mechanical properties are given in Reference 2.

Chemical Composition of Heat No 3P5601
(Weight Percent)

Cr	Ni	Mo	Mn	Cu	Si	C	Fe
2.3	0.2	0.96	0.35	0.03	0.27	0.119	Balance

Creep specimens and low cycle fatigue specimens were machined from the plate with their axes parallel to the rolling direction of the plate. The creep specimens had a 1.27 cm (0.5 in.) diameter by 6.4 cm (2.5 in.) long gauge section with button ends for gripping. Constant load creep testing was carried out on a Satec* Model EE creep frame with a 20:1 load-magnifying lever arm which was self-leveling. Heating was by a resistance tube furnace with temperature control to 1 K. Continuous strain measurements were made using a Satec* Model 200G extensometer with a 5 cm (2 in.) gauge. All tests were conducted at 866 K (1100°F); this was somewhat higher than projected operating temperatures (783 to 811 K), but it allowed time/temperature dependent deformation to occur in reasonable testing times.

*Satec Systems, Inc., Grove City, Pennsylvania.

Initial fatigue tests were conducted in air, but oxidation of the specimen surfaces during long tests with hold periods caused a significant loss of surface material. This made strain measurements inaccurate and decreased the cross-sectional area up to 10 percent. Later tests were run in an argon gas atmosphere.

Stress-strain hysteresis loops were recorded at several intervals, and a continuous output of specimen stress vs time was recorded for each cycle. A decrease in stress at the tensile portion of the loading cycle indicated initiation of one or more fatigue cracks in the specimen.

Several specimens were subjected to constant strain hold periods at their cyclic strain maximum amplitude in either tension, compression, or both tension and compression. The amount of stress relaxation ($\Delta\sigma_r$) during hold was monitored for each case. The total hold time provide approximately 50% creep damage and 50% fatigue damage calculated using a strain range partitioning damage theory [2].

2.2 Results of Creep Testing

The purpose of this test sequence was to generate creep and creep-fatigue damaged samples of 2.25 Cr-1 Mo steel for subsequent destructive and non-destructive examinations. To this end, a variety of test conditions was run to provide extremes of behavior, but no attempt was made to generate a self-contained set of statistically significant mechanical properties data for this alloy. Much of these data has been collected at Oak Ridge National Laboratories (ORNL) and elsewhere.

A summary of results of six creep tests is given in Table 1. The first three tests were conducted in order to apply damage equal

to specified percentages (80%, 40%, and 50%, respectively) of the calculated allowable creep rupture strain specifed in Code Case 1592, (N-47) ASME Boiler and Pressure Vessel Code. The low level of resultant strains demonstrated the conservatism ot the code rules. To produce higher strained material, the stress level was increased for specimen 2.25 Cr-C-4 to a value that was anticipated to produce failure in about 1200 hr., according to data given in Reference 4. Instead, the specimen failed in 119 hr.

An empirical relationship that is better able to predict time to rupture (t_r) was developed by Booker and Hebble [5] at ORNL:

$$\log t_r = 12.4 - 5.10 \times 10^{-3} \quad T + 1.02 \log \sigma - 9.88 \times 10^{-7} \quad T^2 \ (\log \sigma)^2$$

where t_r is rupture time in hours, T is test temperature in degrees Rankine, and σ is the applied stress in thousands of pounds per square inch. This equation predicted about 100 hours for specimen 2.25 Cr-C-4 (in good agreement) and approximately 325 hours for specimens 2.25 Cr-C-5 and -6.

Final creep strain values reported in Table 1 were calculated from changes in gauge diameter. These diametral changes were due to both oxidation and deformation, since oxidation in this steel forms an oxide which flakes off during creep. A measure of the oxidation loss could be made from changes in diameter of the specimen shoulders, which were entirely due to oxidation. This is reported as $\Delta d_{oxidation}$ in Table 1. An equivalent axial engineering strain in the neck was calculated using this relation which assumes constant volume:

$$\epsilon_{axial} = 2\frac{\Delta d}{d_o} = \frac{2\left[d_o - (d_f + |\Delta d_{oxidation}|)\right]}{d_o}$$

where d_o is the inital gauge diameter, d_f is the final diameter without oxide, $\Delta d_{oxidation}$ is diametral change due to oxidation.

The creep specimens, then, provided samples damaged at three stress levels between times of 119 and 804 hours at creep strains from 1% to approximately 11% in necked regions. The failure mode of the one specimen carried to rupture (2.25 Cr-C-4) was by ductile void growth with a necked reduction of area of 92%.

2.3 Results of Creep-Fatigue Testing

Table 2 lists the test conditions and results for the fatigue specimens with and without hold periods. The first specimen (2.25 Cr-MTF-1) at a relatively low total strain range ($\Delta\epsilon$) of 0.5%, had a life of 28011 cycles; a test with this number of cycles with hold times would have lasted too long, so a higher total strain range of 1.0% was selected for the remaining samples.

The legend of Table 2 defines the imposed test variables and the resulting stress and strain levels which describe the stress-strain fatigue hysteresis loops. Figure 1 shows four schematic hysteresis loops with labeled stress levels for (a) no hold period, (b) tensile hold period at constant strain, (c) compressive hold at constant strain, and (d) combined tensile and compressive holds. The reader is referred to Reference 6 for a more complete description of hysteresis loops resulting from elevated temperature fatigue.

The stress range ($\Delta\sigma$) at half life was lower in all but one case than the range at start of test; this cyclic softening suggests a microstructural rearrangement to a state which permits easier dislocation motion. Apparently, small precipitates observed to form during fatigue (discussed in Section 5.4) were not potent strengthening obstacles. Also, hold periods in one stress direction caused a net mean stress in the opposite direction. For instance, specimen 2.25 Cr-MTF-3 had a compressive hold and σ_t is greater than σ_c; specimen 2.25 Cr-MTF-4 had a tensile hold and σ_c is greater than σ_t. For the specimen with equivalent hold times (2.25 Cr-MTF-5) σ_t and σ_c are nearly equal.

Two trends are evident with respect to atmosphere effect on fatigue life. Hold times in air environment experiments strongly decreased the number of cycles to failure or initiation, implying a large creep component of damage. (Compare specimens 2.25 Cr-MTF-2 vs. -3,-4, and -5). However, the two tests with hold times conducted in argon showed large increases in life over equivalent tests conducted in air. (Specimens 2.25 CR-MTF-3 vs. -6 and -4 vs. -7). This indicated that what was thought of as creep component of damage is actually caused by oxidation. This could be due to both oxidation effects in crack initiation and propogation and to changes in cross-sectional area during the experiment. Pure fatigue tests without hold periods showed essentially equivalent life times for air and argon environments, but these tests lasted a relatively short time. (Specimens 2.25 Cr-MTF-2 and -8).

3. Non-Destructive Examination of 2.25 Cr-1 Mo Steel Creep and Fatigue Specimens

3.1 Ultrasonic Velocity Measurements

The ultrasonic longitudinal and shear velocities were determined at room temperature using the pulse overlap technique [7]. Conventional ultrasonic transducers were used with a Dow-Resin 276-V9 couplant between the transducers and the specimen. A 10 MHz 0.6 cm diameter transducer was used to make the longitudinal velocity determinations, and a 5 MHz 1.2 cm diameter transducer was used for the shear velocity measurements.

To measure ultrasonic velocity, the method measures the time between pulse generation and the return of an echo from a back surface. This requires accurate knowledge of specimen thickness. Each specimen was ground with flat and parallel sides to provide a uniform thickness over the total length of the specimen. In this way appropriate velocity measurements were made at locations in the grip sections of the specimens as well as in the gage section of the same specimen. Therefore, the velocity measurements for each specimen at the creep or fatigue-damaged section could be compared with the velocity measurements at the undamaged grip sections of the same specimen. Figure 2 shows five creep specimens with machined flats.

Examination of the fatigue specimens presented special problems. With fractured specimens which were hour-glass in cross-section, the region of maximum damage was always just below the fracture surface. The low volume of this damaged material and its proximity to the fracture surface made it impossible to make measurements of only damaged regions. For this reason, only two specimens which were

fatigued just to crack initiation, removed from the machine, and ground with flats were suitable for ultrasonic velocity measurements.

Shear velocity measurements were taken with the particle motion polarized either parallel or perpendicular to the axial direction of the test specimens. The longitudinal and shear velocities were also measured in the axial direction for three creep specimens (2.25 CC-1, -5 and-6). These measurements were made on small pieces cut with flat and parallel sides from the gage sections of these specimens. Table 3 summarized all the ultrasonic veolcity values measured.

As can be seen from Table 3, there is a small difference in the longitudinal and shear velocities in the undamaged region for the different specimens as well as between the axial and transverse polarization shear velocities of the same specimen. This indicates that a small amount of anisotropy was present in the 2.25 Cr-1 Mo steel plate from which the specimens were made due to preferential crystallographic orientation of the grains in the rolling direction of the plate. The machined flats for each specimen were cut at a random orientation to the thickness direction of the plate so that changes in the ultrasonic velocity at the damaged region could only be compared with the velocity measured in the undamaged region of the same specimen. The experimental error in longitudinal velocity is no larger than $\pm$ 0.004 mm/μsec, and in shear velocity it is no larger than $\pm$ 0.002 mm/μsec.

The only specimens which showed a conclusive change in velocity beyond these errors between the damaged and undamaged regions of the same specimen are creep specimens 2.25 Cr-C-5 and -6 and fatigue specimens 2.25 Cr-MTF-4 and -5. Refer to Tables 1 and 2 for a

listing of strain levels and cycles to failure, respectively, for the creep and fatigue specimens. In creep specimen 2.25 Cr-C-6 the shear velocity polarized axially showed a 0.37% increase in velocity between the necked (11% equivalent strain) and undamaged regions. The shear velocity in this specimen polarized in the transverse direction showed a 0.28% decrease in velocity. In creep specimen 2.25 Cr-C-5 only a small increase of 0.15% was observed in shear velocity polarized in the axial direction; this test was stopped at the onset of necking at a strain of 2.7%.

For the fatigue specimens 2.25 Cr-MTF-4 and -5 the shear velocities polarized axially decreased by 0.37% and 0.12%, respectively, between the damaged and undamaged regions. The shear velocity polarized transversely increased by 0.24% and 0.37%. The direction of velocity change in the fatigue samples was opposite from that measured for the creep samples.

The magnitudes of velocity changes observed for highly damaged regions of both types of tests, while experimentally significant, were very small. For the creep specimens, the size of the effect was dependent on the amount of damage: no change was seen for low creep strains, a small change for intermediate strains (2.7%), and the largest effect for the highly necked sample (11% strain). Comparison of results between the two fatigue specimens showed no definable trends.

These changes in wave velocity are likely due to small directional variations in elastic modulus which occurred because of deformation. During creep, grain elongation occurred, especially in the neck, and this would lead to changes in crystallographic texture. This texture

would cause the modulus to vary with specimen orientation. In fatigue, the texture could have occurred on a finer scale by directional orientation of the subgrains which formed (see section 4). As mentioned previously, differences in longitudinal and shear velocities between different undamaged specimens indicated the presence of texture prior to the tests. Post-test changes would be a rearrangement of the prior texture. A complete explanation of this effect would have required detailed textural measurements by x-ray diffraction, but this was not within the scope of the program.

Since the overall magnitude of the effect was so small, even for nearly ideal laboratory conditions, it was judged unsuitable as a practical volumetric NDE technique to monitor elevated creep-fatigue damage.

3.2 Magnetization Curve and Hysteresis Loop for 2.25 Cr-1 Mo Creep and Fatigue Specimens

The magnetic properties of the creep specimens were examined before and after creep damage occurred by plotting the magnetization and hysteresis curves for each specimen. No observable change in these curves was noted due to creep damage. For example, creep specimen 2.25 Cr-C-6, the remenence was measured to be 618.942 gauss and the coercivity was measured to be 6.660 oersted. The permeability at zero magnetic flux density was calculated to be 92.79 gauss/oersted.

4. Observations by Optical Microscopy

Optical microscopy of the as-received normalized plate of 2.25 Cr-1 Mo steel showed a microstructure made up of approximately 80% proeutectoid ferrite and 20% pearlite. The ferrite grain size averaged 35 μm, and the grains were equiaxed. Figure 3 shows this structure in which the pearlite is the dark area, and the ferrite grains are essentially free of optically resolvable particles.

4.1 Creep Specimens

Long periods at 866 K (1100°F) during the creep test caused two changes: the pearlite lamellae began to spheroidize and a fine precipitate became visible within the ferrite grains. This is discussed further in Section 5 with the TEM observations. Figure 4 shows a view of the gauge section of specimen 2.25 Cr-C-1 which ran for 804 hours. A similar microstructure is evident in the under-formed button end of specimen 2.25 Cr-C-6 (Figure 4a) which lasted 550 hours. Evidence of the approximately 11% axial strain which occurred in the neck of 2.25 Cr-C-6 is shown in Figure 5b (note different magnification). Elongation of the grains in the stress direction is the only indication of plastic strain which was visible by optical microscopy of the creep specimens.

4.2 Fatigue Specimens

The longest fatigue test (2.25 Cr-MTF-6) lasted approximately 300 hours, and this produced aging effects comparable to the creep tests: partial spheroidization of pearlite and growth of a resolvable fine precipitate. For the shorter tests without hold periods, these changes were not observed.

An additional effect noted in the fatigue test was the formation of wavy grain boundaries (see Figure 6a for specimen 2.25 Cr-MTF-6). The spacing of the grain boundary serrations is approximately 2 μm, which is on the order of the fatigue induced subgrain size of 1-2 μm observed by TEM (see section 5.4). Mullendore and Grant [8] have reported that serrations represent intersections of subgrain boundaries with a grain boundary in creep deformed aluminum-magnesium alloys. The serrations result from local rearrangements of grain boundary segments to minimize surface energy. Wavy boundaries appeared in fatigue specimens and not creep specimens in this case because the accumulated strain in fatigue was much greater than in creep.

5. TEM Observation of 2.25 Cr-1 Mo Steel

Changes in microstructure which result from creep or fatigue at 866 K are caused by both the stress-strain history and by the time at high temperature during the test. This section summarizes the TEM observations from several sets of samples. The microstructure of the as-received material is presented first, followed by a discussion of changes caused by zero stress aging at 866 K. The microstructures of specimens deformed by creep or fatigue at 866 K are then compared with the effects of aging.

Samples for TEM examination were sectioned from the test specimens by spark cutting and were ground to about 100 μm thickness using SiC papers. They were then jet electropolished in anhydrous sodium chromate in acetic acid solution at 20 V. Samples were examined in a JEM-100C electron microscope at a 100 KV accelerating potential.

5.1 As-Received Microstructure

As previously noted, optical microscopy showed that the as-received material consisted of two regions: pearlite making up about 20% of the material, and ferrite in which no carbides were resolved. Electron microscopy revealed that carbides were present in all regions of the material as shown in Figure 7. The pearlite of as-received material as shown in Figure 7a, consisted of lamellae of $M_{23}C_6$ Carbides [9] which had about a 0.1 μm spacing and are several μm in length. Figure 7b shows a region of proeutectoid ferrite which contains a fine distribution of carbide precipitates. The majority of these precipitates are rods 0.02 to 0.04 μm thick and 0.5 to 1.0 μm

long which lie along <100> matrix directions. A few precipitates are present which are more idiomorphic and do not appear to form along specific crystallographic directions. Hale [9] has identified the carbide phase which forms in the proeutectoid ferrite on cooling from the austenitizing treatment as Mo_2C. The chemistries of the carbide phases observed were not determined during this study. The microstructures shown in Figure 6 are very similar to those observed by Hale [1] in which the needle shaped carbides were found to be the Mo_2C type. The dislocation density of the steel in the as-received condition was about 10^8 cm^{-2} which is also similar to the dislocation density of the starting material in Hale's study [1].

5.2 Effects of Aging up to 800 hrs. at 866 K (1100°F)

After several thousand hours at temperatures above 866 K (1000°F), the carbides in 2.25 Cr-1 Mo alloy steel were found to be completely spheroidized with a large number of carbide precipitates present at the grain boundaries [10]. Leitnaker, et al, [11] determined that $M_{23}C_6$ tended to be the primary carbide formed, with $M_{23}C_6$ and Mo_2C carbides present in decreasing amounts at longer times.

Figure 8 shows spheroidization and coarsening just beginning after 119 hrs. at 866 K (1100°F). The $M_{23}C_6$ carbide lamellae shown in Figure 8a have begun to break apart and spheroidize while the Mo_2 carbides shown in Figure 8b remain essentially unchanged. The rods of Mo_2C have not changed either in dimension or shape and continue to lie along <100> directions. After 550 hours at 866 K (1100°F), significant changes have finally begun to occur, as Figure 9 shows. Many regions remain very similar to the initial microstructure such as shown in Figure 9a. The only influence of the high temperature

treatment in these areas is a slight increase in the number of non-oriented idiomorphic precipitates. In addition to these relatively unchanged regions, aging 550 hours resulted in extensive coarsening and spheroidization in a few areas. Figure 9b shows an area in which the as-received structure has completely changed. The carbides shown range in size from 0.05 μm to 0.25 μm in diameter. Concurrent with this change in precipitate morphology is a change in the dislocation substructure. Although these specimens did not undergo either creep or fatigue deformation, dislocations in the spheroidized regions tended to be arranged in subgrain walls. Figure 9b shows this process beginning; Figure 9c shows a region which has formed into well defined subgrains.

Aging 804 hours at 866 K (1100°F) produces a continuation of the same changes that were noted after 550 hours. Figure 10a shows that pearlitic regions have not completely spherodized, but the process results in carbide particles which are about 0.05 μm in size. Although the coarsening process continued, some regions remain little changed, as Figure 10b shows. A comparison between Figures 10b and 7b illustrates that, in some regions, 804 hours at 866 K (1100°F) has had no effect on the microstructure. The tendency of some regions in 2.25 Cr-1 Mo alloy steel to resist spheroidization and precipitate coarsening after hundreds of hours at temperatures above 866 K (1100°F) has also been observed by Hale [1]. In that study, examples aged at 866 K (1100°F) for over 10,000 hrs. contained regions of proeutectoid ferrite which included the rod shaped Mo_2C precipitates and appeared unchanged from the starting microstructure.

This work and Hale's [1] work indicate that two stages in aging occur in 2.25 Cr-1 Mo steel above 866 K (1100°F). Initially, spheroidization of the carbide precipitates occurs in widely separated regions of the material and progresses to include an increasing volume as the time at high temperatures increases. During this period, only those regions which have undergone spheroidization show coarsening of the carbides. Eventually, all of the material contains spheroidized carbides and the primary change in microstructure which occurs on continued aging is the coarsening of the carbides both within the matrix and at the grain boundaries.

5.3 Microstructures from Specimens Creep Deformed at 866 K (1100°F)

Three creep-damaged specimens have been examined by transmission electron microscopy: 2.25 Cr-C-1, -4, and -6. Table 1 describes the history and Figures 11 through 13 show the microstructure of each of these samples. It would be very difficult to make direct, sequential comparisons among these specimens since all were tested at different stresses, all were held at 866 K (1100°F) for different times and the tests were stopped at different stages in creep life.

Sample 2.25 Cr-C-1 was tested into Stage 2 creep under 69 MPa (10 ksi) stress to a strain of 1.0%. This test lasted 804 hours and the resulting microstructure is shown in Figure 11. By comparison with Figure 10, it is clear that the material exposed to the 69 MPa (10 ksi) stress does not have a significantly higher density of dislocations than unstrained material. At 866 K (1100°F), it appears that the steady state creep condition is reached with no initial increase in dislocation density during Stage 1. Most of the dislocations in Figure 11 have been pinned at the carbide precipitates.

Sample 2.25 Cr-C-6 was tested into Stage 3 creep under 97 MPa (14 ksi) stress for 550 hours to an equivalent axial strain at the neck of 11%. The microstructures shown in Figure 12 have been taken from the necked region of the sample. Figure 12 shows a region with a precipitate distribution unchanged from the as-received structure, and the dislocation density is only slightly higher after necking in creep than in the as-received material. The areas which have begun to spheroidize and coarsen after 550 hours at 866 K (1100°F) show, as in Figures 12b and 12c, a tendency for the formation of subgrains. Figure 12b shows the process of subgrain formation beginning with dislocation networks developing between several spheroidized carbide particles. In this region, a few of the rod shaped Mo_2 precipitates remain. Figure 12c shows an area in which spheroidization is complete and well defined subgrains have formed that are between 0.5 and 2 μm in size. The magnitude of the crystallographic misorientation between subgrains is evidenced by the differences in contrast among the subgrains in Figure 12c. The formation of subgrains in creep deformed material is very similar to those that formed during simple aging as can be seen by comparing Figures 9 and 12.

Sample 2.25 Cr-C-4 was tested to rupture at a stress of 124 MPa (18 ksi) at 866 K (1100°F); this test lasted 119 hours to failure. Because of the higher stress on this specimen, it failed before significant changes in the carbide precipitate distribution could occur. The areas shown in Figure 13 are from the necked part of the specimen. Figure 13 shows a pearlitic region in which the lamellae are beginning to break apart into smaller particles but

the dislocation density remains low, although subgrain boundaries have formed along the pearlite colony boundaries. A proeutectoid ferrite region is shown in Figure 13 which illustrates that the Mo_2C rods are unchanged from the as-received condition; at the higher load of 124 MPa (18 ksi), however, the dislocation distribution is different. Subgrain boundaries have been formed among the Mo_2C rods as shown in Figure 13b with the dislocation density between the boundaries remaining low.

Hale [1] has observed the microstructures resulting from creep of 2.25 Cr-1 Mo steel at 35 MPa (5 ksi) for temperatures between 843 K and 948 K (1058°F and 1247°F) and attempted to correlate precipitate microstructure to creep deformation stage. His assumption in this approach is that the creep deformation rate and the precipitate coarsening rate are both controlled by the diffusion of vacancies and therefore both processes proceed at a rate defined by energy for vacancy motion. For the stress and temperatures chosen by Hale, both creep and precipitate coarsening do appear to occur at about the same rate. Accordingly, Hale does show that samples tested to the start of Stage 3 creep at different temperatures, and therefore different times, all have similar precipitate distributions. Hale states that this correlation may be limited and this limitation has been shown in this study. Sample 2.25 Cr-C-1 had undergone significant changes in precipitate distribution but was still within Stage 2 creep while sample 2.25 Cr-C-4 showed little change in the precipitate morphology yet the sample had ruptured.

The breakdown of Hale's approach results from a failure of his assumption of equal activation energies for precipitate coarsening and creep deformation. Although there is not complete agreement among investigators, indications are that diffusion of vacancies to jogs is not generally the rate determining feature of steady state creep. Instead, stress assisted, thermally activated glide events may be the rate controlling features [12]. Simplistically, diffusion controlled precipitate coarsening occurs at a rate determined by

$$\text{Rate} \propto [\exp[-E/kT]] \tag{1}$$

where E is approximately the vacancy motion energy. This rate contrasts with the rate at which thermally activated stress assisted dislocation glide events occur:

$$\text{Rate} \propto \exp[-(\sigma-\sigma_i)bA/kT] \tag{2}$$

where σ is the applied stress, σ_i is an internal back stress, b is the Burger's vector and A is the activation area for the process. The only way that the rates of precipitate coarsening and creep deformation will be proportional is if the quantities E and $(\sigma-\sigma_i)bA$ happen to be fortuitously related.

This study has revealed that the variation in the microstructure from region to region within each sample is generally as large as any possible variation in microstructures between samples with greatly different histories. This situation makes the assignment of a single value for such parameters as dislocation density or precipitate size and spacing very difficult. A more meaningful quantitative characterization of the changes in microstructure would be a measure

of the volume fraction of proeutectoid ferrite which has undergone spheroidization as a function of time and temperature. These measurements would require large amounts of viewing time on the electron microscope and have not been made during this study.

5.4 Fatigue Deformation at 866 K (1100°F)

Of the fatigue and creep/fatigue tested specimens described in Table 2, sections of 2.25 Cr-MTF-1, -6 and -8 have been examined by transmission electron microscopy. The selection of these sections allows two pertinent comparisons to be made. First, the relationship between the microstructures of 2.25 Cr-1 Mo steel cycled at two different strain ranges, 2.25 Cr-MTF-1 and -6 can be studied. Second, the effect of a 6 minute compressive hold time can be examined by comparing 2.25 Cr-MTF-6 and -8.

Figure 14 shows the microstructures which result from cycling to failure at a total strain range of 0.5% in a test which lasted 28011 cycles and 19.4 hours. It is evident from Figure 14 that cyclic deformation produces changes in the precipitate distribution which do not occur during simple aging at 866 K (1100°F). Figure 14a shows a region of proeutectoid ferrite which contains a large number of spherical precipitates which form heterogeneously along dislocations in addition to the rod shaped Mo_2C carbides that are present in the starting material. Dark field TEM shows that the 0.03 μm diameter spheres are second phase precipitates, probably carbides, but the exact composition or crystal structure has not been determined. In several places, these small precipitates form in bands

of particles, as shown in Figure 14b, which are about 0.08 μm wide and separated by about 0.16 μm. An indication that these precipitates are carbides is their absence in the solute depleted zones adjacent to the carbide particles which were present in the starting material. The total dislocation density in the proeutectoid regions is higher than in the as-received material; however, many of the dislocations are immobile due to pinning by the precipitates which form during testing. Figure 14c shows a pearlitic region in which subgrain boundaries have formed at the pearlite colony boundaries. Precipitation during testing is not as prevalent in these areas, although a fine scale precipitate formed in the few places where the distance between $M_{23}C_6$ lamellae is greater than 0.35 μm.

The 2.25 Cr-MTF-8 sample was cycled at the larger total strain range of 1.0% with failure occurring after 1810 cycles and 2.52 hours. Figure 15 shows that after only several hours of testing, the precipitation process has not yet begun in some areas (Figure 15b) and has only just started in other areas (Figure 15a). Subgrain formation has occurred in regions such as shown in Figure 15b where the dislocations have not been pinned by small percipitates. In regions where these precipitates have formed, the subgrain walls are only beginning to appear. These precipitates are less than 0.02 μm in diameter and are not always associated with dislocations. An important feature to note in Figure 15a is the tendency for the rod shaped Mo_2C particles to be broken and subdivided into fine particles which are also about 0.02 μm in diameter.

The 6 minute compressive hold time incorporated in the 2.25 Cr-MTF-6 test increased the cycles to failure from 1810 to 2968 and greatly increased the time of the test from 2.4 hours to 301 hours. This longer testing period resulted in extensive precipitation during the test as shown in Figure 16. Extensive subgrain formation is evident in most regions; Figure 16 shows the structure of a subgrain boundary very clearly. Most of the dislocations not associated with the subgrain boundaries are heavily decorated with the spherical precipitates which are about 0.03 μm in diameter. After 301 hours, almost all of the rod shaped Mo_2C carbides have broken up.

Thus, two processes predominate in the microstructural changes which occur during high temperature fatigue. First, small spherical precipitates form, many of them heterogeneously at dislocations, and, second, subgrain boundaries form from dislocations not associated with the small precipitates.

6. Summary of Volumetric NDE on Creep-Fatigue Damaged 2.25 Cr-1 Mo Steel

None of the NDE methods attempted in this study (ultrasonic techniques and magnetization measurements) were successful in continuously monitoring volumetric creep-fatigue damage. However, the destructive TEM observations did provide information on microstructural changes which occur during aging, creep, and fatigue; changes that would have to be measurable by any NDE technique for it to be practical. TEM showed variations in precipitate distribution and morphology and in the dislocation substructure; these variations did not occur homogeneously throughout the samples.

Ultrasonic velocity measurements employed here were only sensitive to changes in modulus and density since:

$$v \propto \sqrt{E/\rho}$$

where v is wave velocity, E is elastic modulus, and ρ is density. These varied too little to cause significant changes in v. Ultrasonic attenuation measurements possibly could be effective if the wave length were approximately the dislocation cell size. However, this requires a frequency of the order of 6000 MHz - two orders of magnitude higher than the 50 MHz currently available. Initial measurements at 10 MHz showed no difference between damaged and undamaged samples. A series of these experiments is currently being conducted here on 316 stainless steel at frequencies up to 50 MHz.

One NDE method which is able to measure dislocation densities is positron annihilation (PA). Currently this technique for 316 stainless steel fatigued at room temperature and at 866 K (1100°F) is being explored. It does not appear that PA measurements can distinguish between cellular and random dislocation structures.

X-ray diffraction techniques can, in principle, be used to measure dislocation density and cell size. These methods are, however, experimentally difficult, and the magnitude of the effects is known to be small.

A major problem inherent with any volumetric NDE technique is relating the measured output to some amount of damage or fraction of component life. TEM observations made here show that microstructural changes are many times not large, and at high temperatures especially, deformation-induced changes may anneal out with time. Current work with dislocation density measurements by positron annihilation on 316 fatigued at room temperature shows that changes in dislocation density may saturate early in the fatigue life so that readings cannot be unambiguously related to life fraction. In addition, fatigue is in reality a process of crack initiation and propagation so that meaningful volumetric readings would have to be made in regions of maximum strain concentration where cracks occur. Any volumetric NDE output must be correlated to some crack initiation criteria, and these criteria have not been experimentally determined.

7. Conclusions

1. Creep-fatigue tests with hold periods lasted longer when tested in argon gas than when tested in air. The effects of oxidation appeared to be at least as great as hold time effects in reducing cycles to failure.
2. Only a small change in ultrasonic shear velocity (0.37%) was observed due to large amounts of creep strain (11%) in the neck of a specimen. The same magnitude change was observed in fatigued samples close to failure.
3. Measurements of magnetization and hysteresis curves on creep damaged specimens showed no observable changes.
4. Qualitative evidence of aging effects and deformation were observed by optical microscopy. Creep deformation to high strains was marked by changes in grain shape, while cyclic straining in fatigue showed up as wavy ferritic grain boundaries.
5. In 2.25 Cr-1 Mo steel, microstructural changes which occur at temperatures above 866 K (1110°F) do not occur homogeneously throughout the matrix. On simple aging and during high temperature creep, carbide spheroidization and coarsening begins in widely separated regions with an increasing volume fraction of the material undergoing these processes as time increases.
6. An imposed creep load does not affect the changes which occur in the precipitate microstructure at high temperatures. Material held at 866 K (1100°F) for 804 hours has the same

precipitate distribution as material under a 69 MPa (10 ksi) creep load for the same time. This is not true of samples which have undergone fatigue tests. Cycling for 2.4 hours produces a precipitate distribution which is clearly different than material simply aged for 2.4 hours. Small precipitates form during fatigue cycling which are not observed to result from aging.

7. Neither creep nor fatigue at 866 K appears to result in high dislocation density substructures. The dislocation substructure after creep deformation is indistinguishable from microstructures resulting from thermal aging alone for a like time period. Fatigue cycling does produce a subgrain microstructure in many regions with the total dislocation density remaining relatively low.

TABLE 1

Summary of Creep Tests: 2.25 Cr - 1 Mo Specimens

(All Tests at 866 K [1100°F])

Specimen No.	Stress MPa(Ksi)	Time (hr)	d_o (mm)	d_f (mm)	$\Delta d_{oxidation}$ (mm)	ϵ_{axial} (%)	Remarks
2.25Cr-C-1	69(10)	804	12.83	12.65	0.05	1.9	Stage 2
2.25Cr-C-2	69(10)	425	12.83	12.70	0.05	1.2	Stage 2
2.25Cr-C-3	69(10)	524	12.83	12.75	0.05	0.4	Stage 2
2.25Cr-C-4	124(18)	119	12.83	12.37	0.02	6.7	Ruptured
2.25Cr-C-5	97(14)	354	12.83	12.62	0.02	2.7	Stage 3 Necking Strain 11%
2.25Cr-C-6	97(14)	550	12.83	12.60	0.02	3.2	Stage 3

TABLE 2

Low Cycle Fatigue Data Summary Table for 2.25 Cr-1 Mo Steel Specimens Tested at 866 K (1100°F)

Spec. No.	$\Delta\varepsilon$ %	Hold Period Tnsn. min.	Hold Period Cmpr. min.	$\Delta\sigma$ at Start MPa	$\Delta\varepsilon_p$ Meas. at Start %	---------at one-half of test duration--------- $\Delta\sigma$ MPa	$\Delta\sigma_r$ MPa	σ_t MPa	σ_{tr} MPa	$\lvert\sigma_c\rvert$ MPa	$\lvert\sigma_{cr}\rvert$ MPa	$\Delta\varepsilon_e$ %	$\Delta\varepsilon_p$ calc %	$\Delta\varepsilon_p$ meas %	N_i cycles	N_f cycles	N_f minutes	Remarks:
2.25 Cr-MTF-1[1]	0.5	-	-	475	.22	414	-	206	-	208	-	.24	.26	.25	25611	28011	1167.12	Failed @ temp.
2.25 Cr-MTF-2[1]	1.0	-	-	545	.68	501	-	248	-	253	-	.30	.70	.69	1691	2000	175.0	Failed @ temp.
2.25 Cr-MTF-3[1]	1.0	-	6.0	570	.72	475	371	246	-	229	125	.22	.78	.79	658	1372	8347.0	Failed @ temp.
2.25 Cr-MTF-4[1]	1.0	6.0	-	495	.74	477	369	227	114	250	-	.22	.78	.79	452	-No N_f-		STOPPED TEST.
2.25 Cr-MTF-5[1]	1.0	3.0	3.0	500	.75	475	290	235	145	240	154	.18	.82	.84	411	-No N_f-		STOPPED TEST.
2.25 Cr-MTF-6[2]	1.0	-	6.0	543	.72	527	424	259	-	268	165	.25	.75	.77	2138	2468	18045.4	Failed @ temp.
2.25 Cr-MTF-7[2]	1.0	6.0	-	506	.70	530	426	246	141	284	-	.25	.75	.77	986	1715	10427.0	Failed @ temp.
2.25 Cr-MTF-8[2]	1.0	-	-	564	.69	523	-	256	-	267	-	.31	.69	.72	1414	1810	150.8	Failed @ temp.

LEGEND:

σ_t = max tensile stress

σ_c = max compressive stress

σ_{cr} = stress level after compressive hold

σ_{tr} = stress level after tensile hold

$\Delta\sigma = \sigma_t - |\sigma_c|$

$\Delta\sigma_r = \sigma_{tr} - |\sigma_c|$, for tensile hold only

$\Delta\sigma_r = |\sigma_{cr}| - \sigma_t$, for compressive hold only

$\Delta\sigma_r = \sigma_{tr} - |\sigma_{cr}|$, for compressive plus tensile hold

$\Delta\varepsilon_e$ = elastic strain range

$\Delta\varepsilon_p$ = plastic strain range

$\Delta\varepsilon = \Delta\varepsilon_e + \Delta\varepsilon_p$ = total strain range

N_i = cycles to crack initiation

N_f = cycles to failure

[1] Tested in air environment

[2] Tested in argon environment

$\dot{\varepsilon} = 4 \times 10^{-3}$ 1/sec

TABLE 3

Summary of Ultrasonic Velocity Values on Creep and Fatigue Specimens of 2.25 Cr-. Mo Steel*

Specimen	Propagation Direction	Velocity Value mm/μsec					
		Longitudinal		Shear Axial		Shear Transverse	
		Undamaged	Damaged	Undamaged	Damaged	Undamaged	Damaged
2.25 Cr-C-1	Transverse	5.940	5.942	3.261	3.260	3.266	3.266
	Axial	---	5.969	---	---	---	3.259
2.25 Cr-C-2	Transverse	5.952	5.952	3.257	3.258	3.253	3.256
2.25 Cr-C-3	Transverse	5.944	5.945	3.255	3.256	3.265	3.265
2.25 Cr-C-5	Transverse	5.947	5.948	3.255	3.260	3.257	3.255
	Axial	---	5.964	---	---	---	3.264
2.25 Cr-C-6	Transverse	5.952	5.947	3.264	3.276	3.269	3.260
	Axial	---	5.966	---	---	---	3.261
2.25 Cr-MTF-4	Transverse	5.957	5.961	3.261	3.249	3.261	3.269
2.25 Cr-MTF-5	Tranverse	5.959	5.966	3.265	3.261	3.265	3.277

*Refer to Tables 1 and 2 for test conditions of creep and fatigue specimens, respectively.

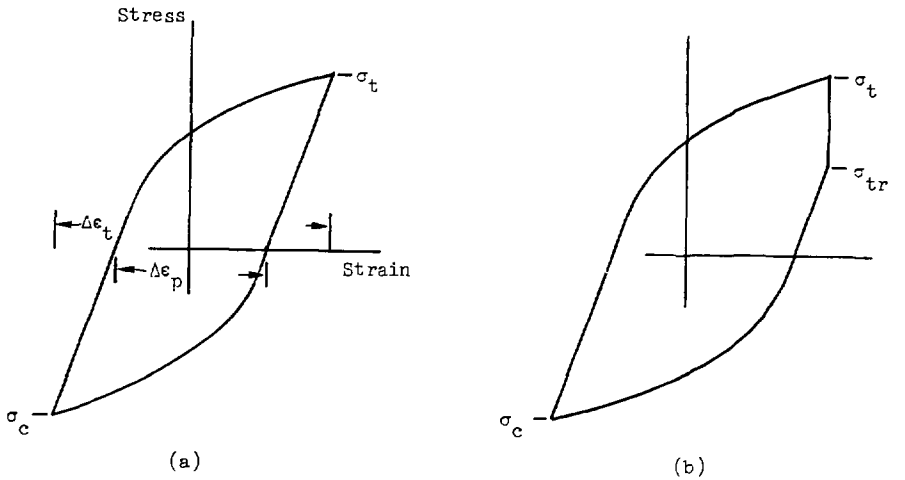

Figure 1

Stress-strain hysteresis loops in strain-controlled fatigue: (a) no hold period, (b) tensile hold period at constant strain, (c) compressive hold period at constant strain, and (d) combined tensile and compressive hold periods.

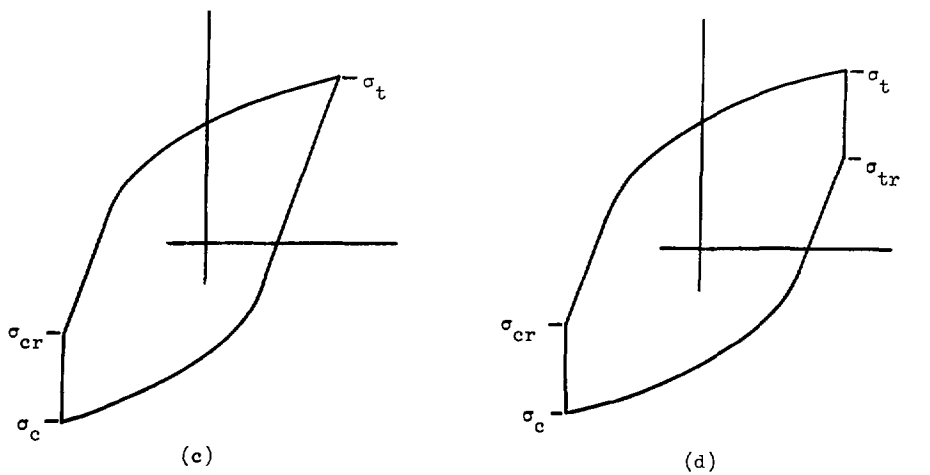

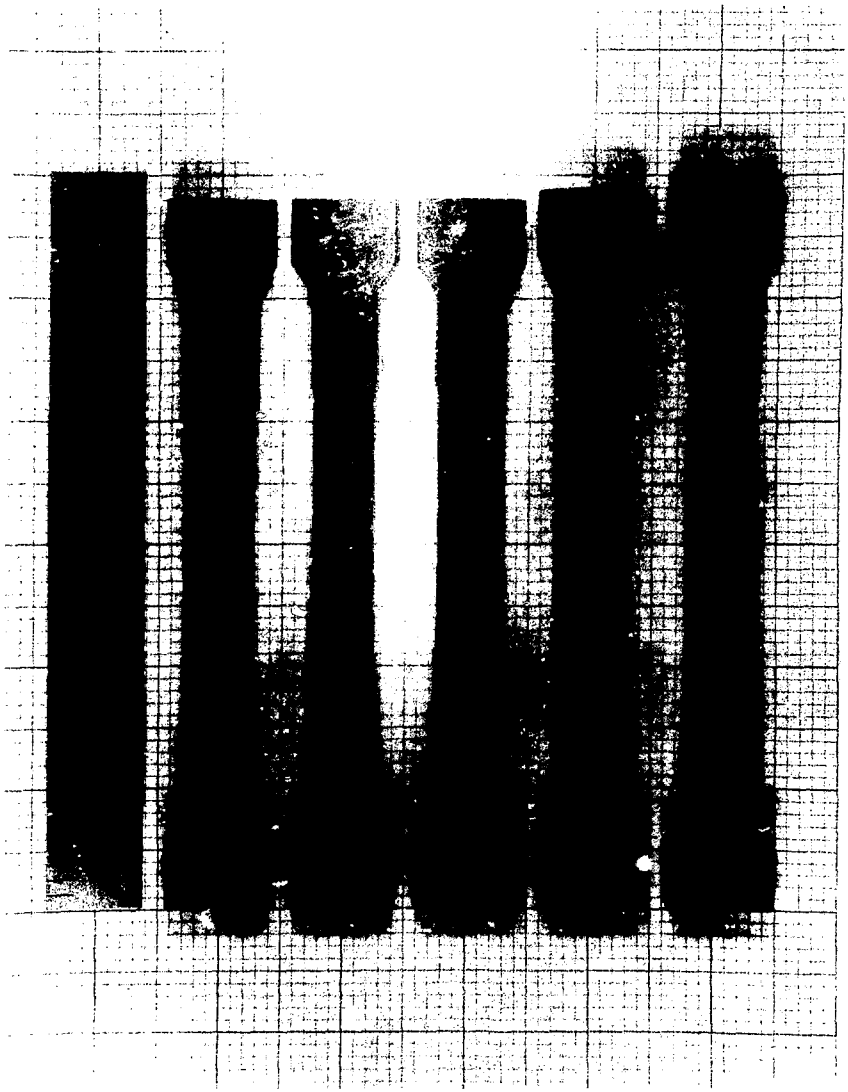

Figure 2. Five 2.25 Cr-1 Mo Steel Specimens with Machined Flats for Ultrasonic Velocity Measurements.

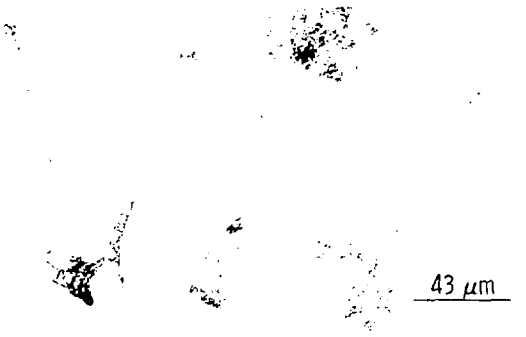

Figure 3. Microstructure of As-received [illegible] Up and Down. 2% Nital Etch.

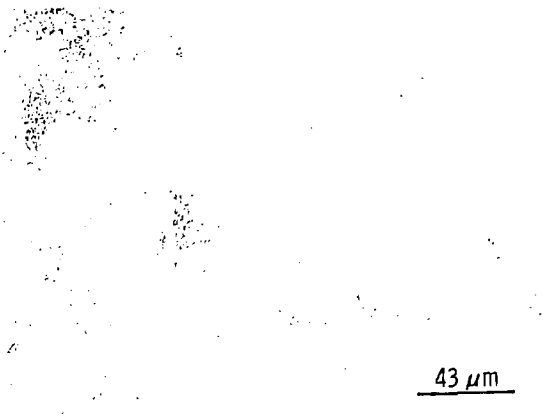

Figure 4. Microstructure of Gauge Section of Creep Specimen [illegible] Cr-C-1 (60 MPa, 866 K, 80h hr., 2% Nital Etch).

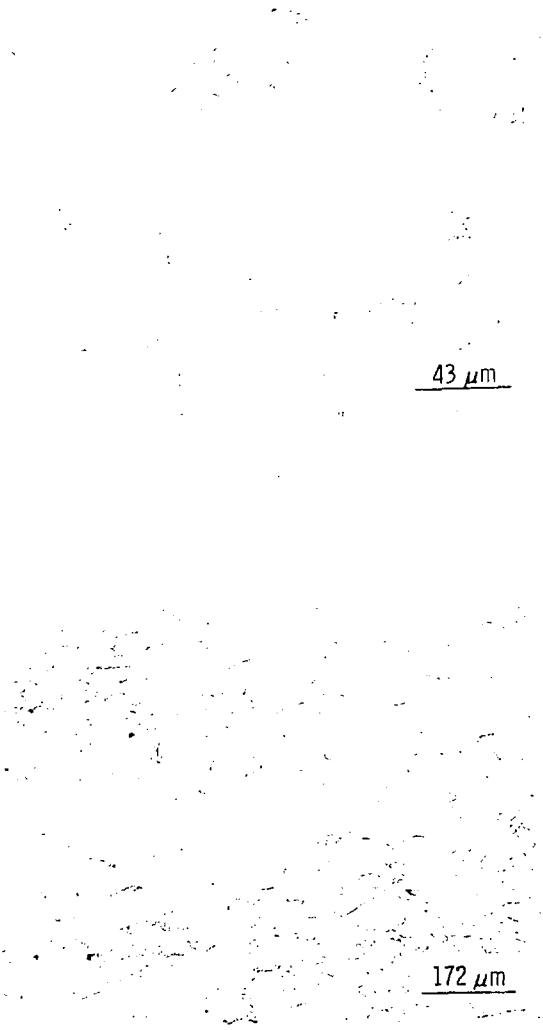

(b)

Figure 5. Microstructure of Creep Specimen 2.25% Cr-0-Cu, 207 MPa, 800 K, 500 hr., 2% Nital Etch); (a - unnumbered button end; (b - necked region, stress direction vice to view.

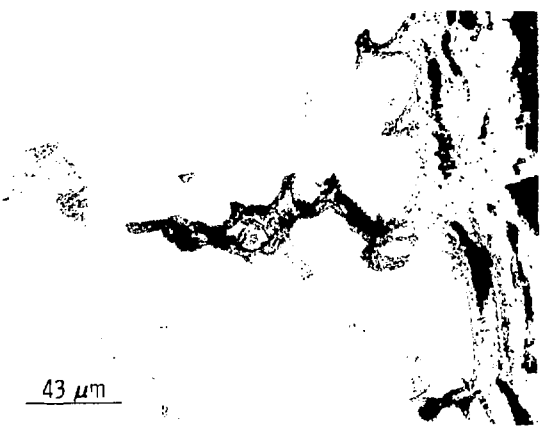

(b)

Figure 6. Microstructure of Fatigue Specimen 2.25 Cr-MTF-6 (2% Nital Etch); 6a - structure just below fracture surface; 6b - secondary crack growing in from the specimen side.

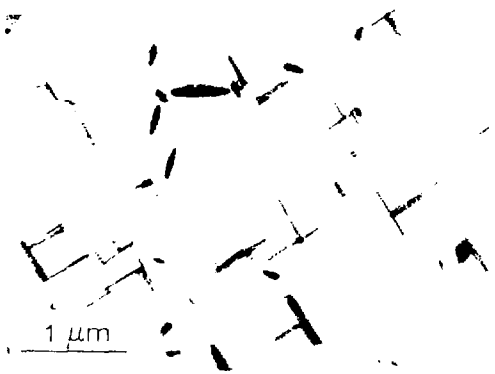

(b)

Figure 7. Electron Micrographs of the As-Received 2.25 Cr-1 Mo Alloy Steel. (a) Bainitic Region; (b) Proeutectoid Ferrite Region.

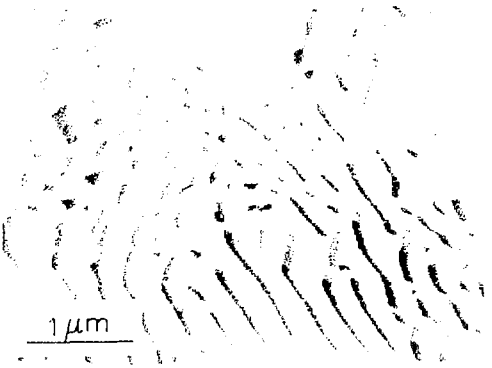

(a)

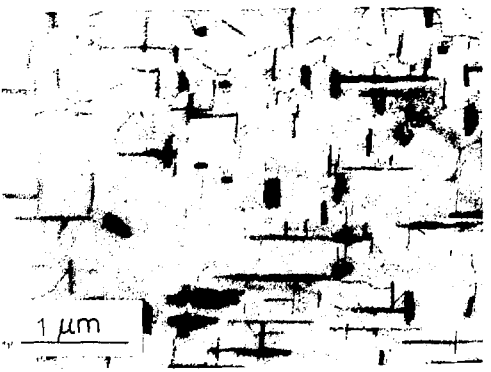

(b)

Figure 8. Microstructure Resulting from 119 Hours at 866 K. (a) Pearlitic Region; (b) Proeutectoid Ferrite Region.

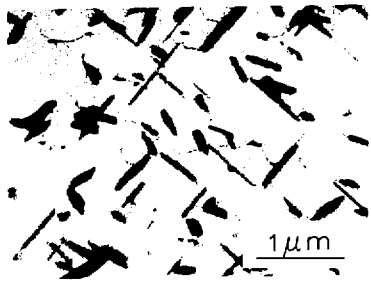

(a)

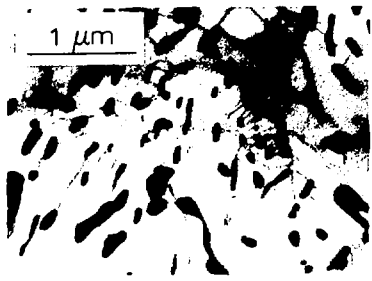

(b)

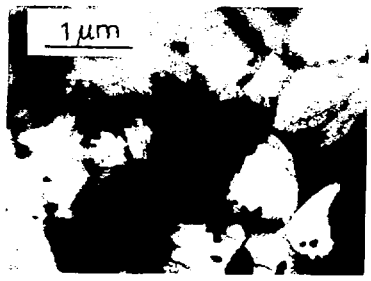

(c)

Figure 9. Microstructure Resulting from 550 Hours at 866 K. (a) Unchanged Proeutectoid Ferrite Region; (b) Region of Carbide Spheroidization; (c) Region Containing Well-Defined Subgrains.

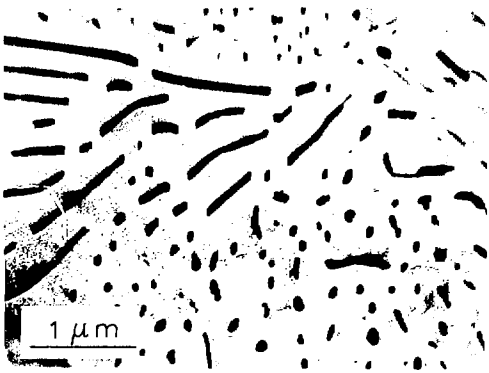

(a)

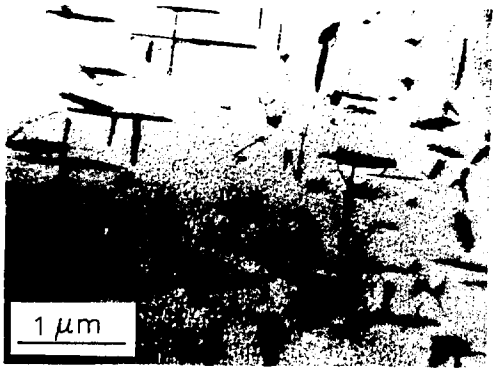

(b)

Figure 10. Microstructure Resulting from 804 Hours at 866 K. (a) Pearlitic Region; (b) Proeutectoid Ferrite Region.

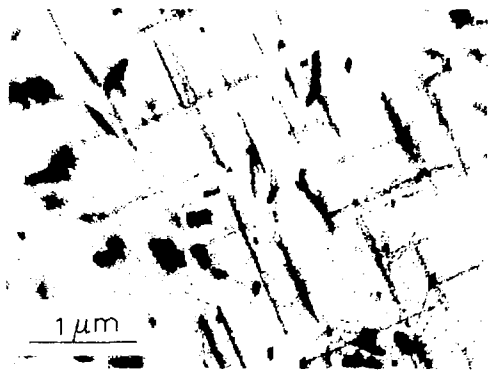

(a)

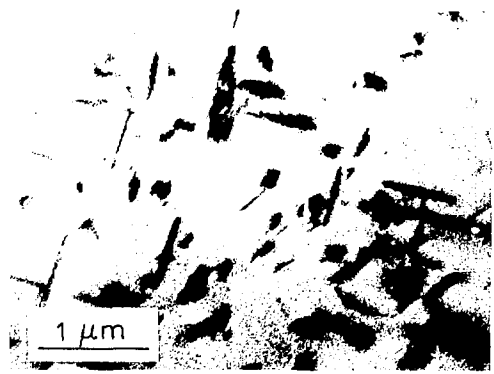

(b)

Figure 11. Microstructure Produced by Creep at 69 MPa for 804 Hours at 866 K. This Test was Stopped in Stage 2 Creep. (a) and (b) Proeutectoid Ferrite Regions.

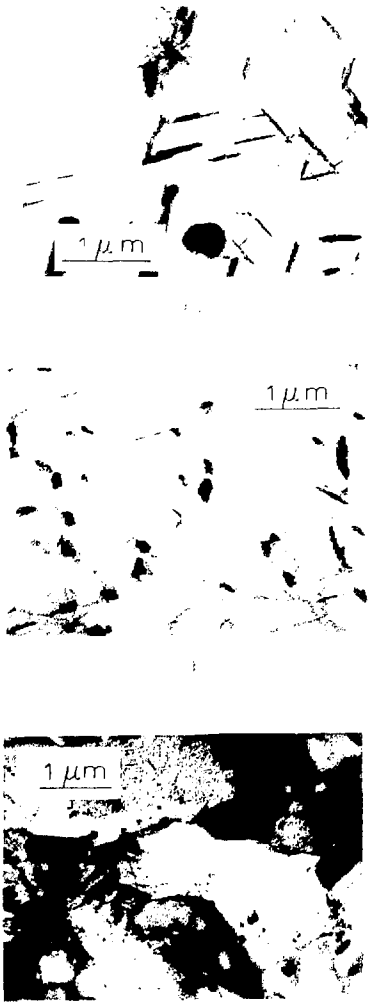

(c)

Figure 12. Microstructure Produced by Creep at 97 MPa for 150 Hours at 866 K. This Test was Stopped in Stage 3 Creep.

(a)

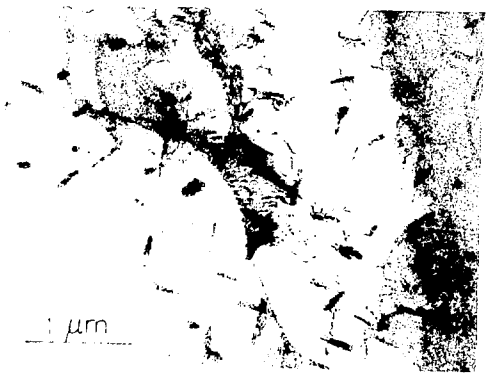

(b)

Figure 13. Microstructure After Rupture Caused by a 1.5 MPa Load for 114 Hours at 866 K. (a) Pearlitic Region; (b) Proeutectoid Ferrite Region.

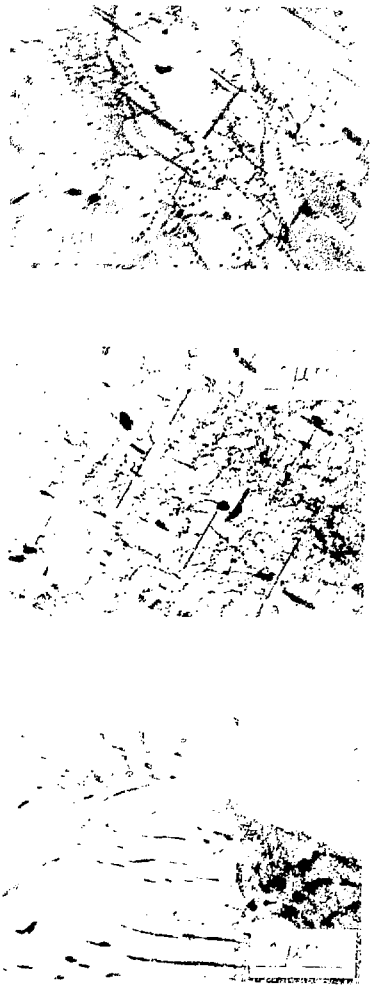

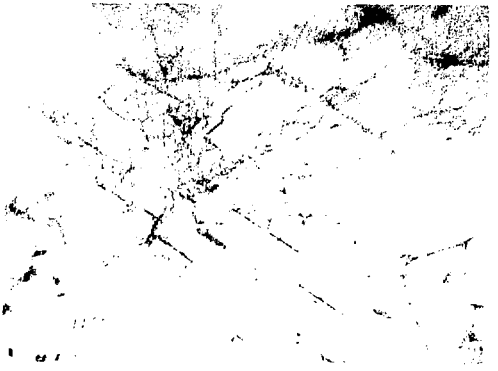

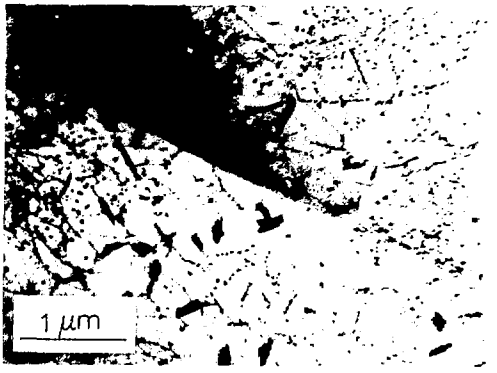

(a)

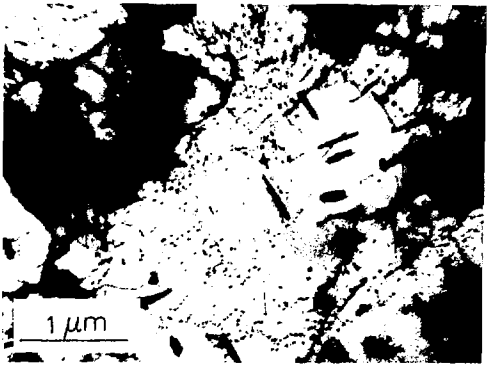

(b)

Figure 16. Microstructure of a Specimen Fatigued to Failure Between ± 0.5% Strain Limits with a 6 Minute Compressive Hold Time. The Test Lasted 2968 Cycles and 301 Hours.

REFERENCES

1. K. F. Hale, "Creep Fatigue Prediction from Observation of Microstructure in 2 Cr-1% Mo Steel," Physical Metallurgy of Reactor Fuel Elements, The Metals Society, London, 1974, pp. 193-201.

2. R. E. Nickell, "Nondestructive Evaluation of Creep-Fatigue Damage--An Interim Report," SAND-77-0076, Sandia Laboratories, Albuquerque, New Mexico, Feb. 1977.

3. J. A. Van Den Avyle, "Elevated Temperature Creep and Fatigue Damage of a 2.25 Cr-1 Mo Steel Weldment," SAND-77-1556, Sandia Laboratories, Albuquerque New Mexico, January 1978.

4. H. G. Edmunds and D. J. White, "Observations of the Effect of Creep Relaxation on High Strain Fatigue," J. Mech. Engr. Sci., Vol. 8, No. 3, p. 310, 1966.

5. M. K. Booker and T. L. Hebble, "Mechanical Properties Correlations of 2-Cr-1 Mo Steel for LMFBR Steam Generator," in Mechanical Properties Test Data for Structural Materials, Quarterly Progress Report for Period Ending October 31, 1974, ORNL-5103, compiled by M. R. Hill, pp. 232-236, December 1974.

6. M. H. Hirschberg and G. R. Halford, "Use of Strain-range Partitioning to Predict High-Temperature Low-Cycle Fatigue Life," NASA; TN-D8072, Jan. 1976.

7. E. P. Papadakis, J. Acoust. Soc. of Amer., 42, pp. 1051 (1967).

8. A. W. Mullendore and N. J. Grant, "Grain-Boundary Behavior in High-Temperature Deformation," Deformation and Fracture at Elevated Temperatures, N. J. Grant and A. W. Mullendore, eds, MIT Press, Cambridge, Mass, 1965, p. 193.

9. K. F. Hale, Proceedings of 4th Int. Conf. on Electron Microscopy, (Springer-Verlag, Berlin, 1960) pp 650-8.

10. R. H. Hiltz, L. H. Kirschler, MSA Research Corporation Report MSAR 69-139 (1969).

11. J. M. Leitnaker, R. L. Klueh, W. R. Laing, Met. Trans. A, 6A, 1949 (1975).

12. W. Blum, Zeit. fur Metall., 68, 484 (1977).

13. W. B. Gauster, W. B. Jones, J. A. Van Den Avyle, and W. R. Wampler, "A Study of Room-Temperature Deformation and Fatigue of 316 Stainless Steel by Positron Annihilation," SAND-77-1570, Sandia Laboratories, Albuquerque, New Mexico, May 1978.